Making it stick: convection, reaction and diffusion in surface-based biosensors

Todd M Squires[1], Robert J Messinger[1] & Scott R Manalis[2]

The past decade has seen researchers develop and apply novel technologies for biomolecular detection, at times approaching hard limits imposed by physics and chemistry. In nearly all sensors, the transport of target molecules to the sensor can play as critical a role as the chemical reaction itself in governing binding kinetics, and ultimately performance. Yet rarely does an analysis of the interplay between diffusion, convection and reaction motivate experimental design or interpretation. Here we develop a physically intuitive and practical understanding of analyte transport for researchers who develop and employ biosensors based on surface capture. We explore the qualitatively distinct behaviors that result, develop rules of thumb to quickly determine how a given system will behave, and derive order-of-magnitude estimates for fundamental quantities of interest, such as fluxes, collection rates and equilibration times. We pay particular attention to collection limits for micro- and nanoscale sensors, and highlight unexplained discrepancies between reported values and theoretical limits.

A wide range of measurements in the life sciences require analytes in solution to react with receptors on a surface. For example, DNA and protein microarrays[1,2], which capture specific genetic sequences and proteins, are ubiquitous in drug discovery and systems biology applications; label-free technologies, such as surface plasmon resonance (SPR) sensors (e.g., Biacore), monitor binding in real time and are used to measure binding affinity[3,4]; and immunoassays based on protein capture are used routinely for medical diagnostics[5,6]. In many situations, it is desirable to quantify surface binding within small fluid volumes to analyze precious samples or to make a large number of measurements from a single sample.

To address these needs, researchers are exploring miniaturized sensors to achieve rapid, sensitive, label-free and small-volume analysis. Examples on the microscale include microcantilevers that translate biomolecular interactions into mechanical bending[7,8], silicon field-effect sensors that measure intrinsic biomolecular charge[9–11], electrochemical sensors that translate biomolecular adsorption to changes in redox current[12,13] and microchannel resonators for measuring mass[14].

Sensors on the nanoscale, such as silicon nanowires[15,16], require far fewer target molecules, and protein detection on the femtomolar level has been reported[17,18]. Recently, sub-femtomolar detection with single-molecule resolution was achieved with a micron-sized optical cavity resonator[19]. Irrespective of the sensing modality, microfluidic systems are of great importance as they provide efficient delivery of target molecules to the sensor surface[20] and enable a high degree of automation[21].

As sensing pushes into such extremes of size and concentration, it is natural to ask whether and when fundamental physical limits will take over. With extremely dilute solutions, how long will the first target molecule take to bind? How many will eventually bind? Can one extract kinetic parameters from measured binding rates? How can one design a system to detect a target molecule most quickly? Can one design a system to bind every target molecule, if they are extremely rare?

Indeed, a variety of recent papers have asked these questions. For example, Sheehan and Whitman[22] theoretically examined diffusive transport of target molecules to small sensors, and argued that sub-picomolar concentration detection using nanoscale sensors would require impractically long time scales (hours to days). On the basis of numerical calculations, they further concluded that flow would help only marginally with small sensors. By contrast, experiments with nanowires show a clear signal within seconds to minutes after ∼10-fM target solutions are introduced[17,18]. Can these results be reconciled?

An important difficulty is that these systems exhibit an extremely rich and varied set of behaviors, with multiple effects competing for dominance. Target molecules diffuse randomly within the solution and are convected along with flowing solutions, free target molecules may chemically bind to an adjacent surface, and bound target molecules may unbind to reenter solution. At least eight (dimensional) parameters are required to describe any such system, and different systems will generally behave in ways that vary substantially, both quantitatively and qualitatively. Exact solutions are not available for any but the simplest of systems, and numerical computations developed for one system are only useful for a second system if the two are analogous in a meaningful way. Advanced mathematical techniques were developed during the past century to handle these kinds of problems[23,24], but require extensive mathematical training. The chemical engineering community has grappled with these problems, as reaction engineering with heterogeneous (wall-bound) catalysts requires one to understand systems in which convection, diffusion and reactions all occur[25–27].

A central goal of this article, then, is to provide a physically intuitive description of these competing physical processes and how they drive

[1]Department of Chemical Engineering, University of California, Santa Barbara, California 93106, USA. [2]Departments of Biological and Mechanical Engineering, Massachusetts Institute of Technology, 77 Massachusetts Ave., E15-422, Cambridge, Massachusetts 02139, USA. Correspondence should be addressed to T.M.S. (squires@engineering.ucsb.edu).

target transport within biosensors of various sizes. Detailed solutions are always required to interpret results in a fully quantitative fashion; however, if one can not say anything about one's system without a sophisticated numerical computation, then it will be difficult to design, optimize or work around bottlenecks. Computers and algorithms may be getting faster, cheaper and easier, but they simply cannot handle a blind search through the eight-or-more-dimensional parameter space. We thus aim to motivate and develop effective 'rules of thumb' that quickly determine in which qualitative behavioral regime a system will operate (e.g., reaction limited versus diffusion limited, rapid collection versus full retention) and thus to develop robust approximate relations that convey how various quantities scale as parameters change. More generally, we hope that this article will serve to bridge two largely distinct communities: those developing and employing new biotechnologies, and those who have developed and mastered techniques for understanding these physicochemical effects (albeit in the context of different systems).

Before beginning, however, we would like to dwell on the obvious. Nothing can be large except by comparison with something else. A retrovirus is too small to see, yet is enormous from an atomic standpoint. Similarly, flows are neither fast nor slow, solutions neither concentrated nor dilute, and sensors neither big nor small without standards for comparison. Meaningful 'apples to apples' comparisons can be made only between quantities with the same physical units—for example, length versus length. The (dimensionless) ratios of two effects under comparison are incredibly informative and play an extremely important role in the study of fluids and transport. Fluid mechanics is replete with dimensionless numbers; those most pertinent to microfluidics have been recently reviewed and explored by Squires and Quake[28].

In what follows, we examine the effects of convection, diffusion and reactions through a paradigmatic model system (**Fig. 1**), with the idea of providing a comprehensive and unifying treatment of these competing effects. Target solution flows with volumetric flow rate Q through a channel of height H and width W_c, one wall of which contains a sensor of width W_s, and length L in the flow direction. The sensor is functionalized with b_m receptors per unit area, and the solution contains target molecules with concentration c_0, and diffusivity D. For simplicity, we assume that target molecules in solution only bind receptors on the sensor with binding constants k_{on} and k_{off}, and do not bind to the sensor substrate. Because channel widths W_c are typically much larger than heights H, we assume concentrations to be uniform across the channel (in the H direction). As such, all numerical computations and most scaling arguments presented are two-dimensional, and we identify cases when this approximation may fail.

This system is the simplest one that contains all of the relevant ingredients—and yet it is not at all simple. We emphasize approximate scaling solutions that give order-of-magnitude estimates for behaviors (e.g., binding time) and how they scale as parameters (e.g., flow rates, concentration or geometry) are varied. Five relevant dimensionless parameters arise naturally and intuitively for this system, various values of which give rise to qualitatively different behavioral regimes. We complement these intuitive pictures and semiquantitative scaling arguments with finite-element computations using Matlab and COMSOL to both support and extend our results. Our presentation is meant to appeal to intuition, and details about the governing equations and details of the simulations we perform can be found in the **Supplementary Notes** online. (In particular, see **Supplementary Figure 1** for a definition sketch for the computations.)
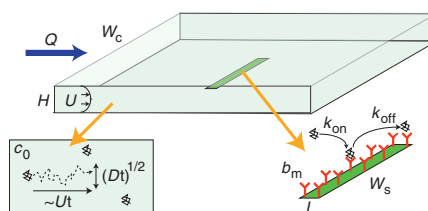

Figure 1 Model system studied here. Solution with target concentration c_0 flows with velocity U and volumetric flow rate $Q \sim HW_cU$ through a channel of height H and width W_c over a sensor of length L and width W_s that is functionalized with b_m receptors per unit area. The kinetic rate constants for the (first-order) binding reaction are k_{on} and k_{off}, and the diffusivity of the target molecules is D.

Random walks

To build this intuition, we start with the simplest possible sensing system: target molecules that diffusively wander through solution and bind immediately upon encountering the sensor. As Sheehan and others have argued[22], this 'perfect collection' case represents the ultimate collection limit for nonconvective systems—finite reaction rates only slow down binding.

Diffusion involves random and uncorrelated steps, giving target molecule displacement that does not grow linearly in time, but like the square root of time (see ref. 29 for an intuitive, biologically inspired introduction). The time for a target molecule to diffusively reach a sensor thus scales statistically like the square of its distance away. Rather than treating and tracking individual target molecules, each taking independent and random steps, one can describe collections of individual target molecules statistically. This approach yields a concentration field c that represents an ensemble average of the stochastic behavior of individual target molecules, as would be obtained by averaging many single-molecule experiments (or simulations). This ensemble average is naturally reproduced by concentrated solutions, which involve a great many target molecules acting simultaneously within the relevant experimental window. Experiments with extremely dilute solutions, on the other hand, may contain too few target molecules to resemble this ensemble average at any given time. For example, a femtomolar solution contains about one target molecule per nanoliter (that is, per cube of size 100 μm). At any given time, concentration profiles measured in, for example, femtomolar solutions will appear grainy on these length scales (e.g., in any microfluidic experiment) and will thus not seem to resemble the smooth profiles presented here. However, averaging the results of many such experiments or simulations would, indeed, yield the smoothly varying concentration fields depicted and described in this article.

Figure 2 shows the behavior of this ideal sensor. As target molecules are collected by the sensor, a depleted zone forms with 'size' $\delta \sim \sqrt{Dt}$. The depletion zone starts relatively flat (**Fig. 2a**), until its thickness δ becomes comparable to the sensor size L (after time L^2/D). It then grows radially for a time scale $\tau_D = H^2/D$ until it spans the channel (**Fig. 2b**), after which it extends into the channels, with a length $\delta \sim \sqrt{Dt}$ that grows indefinitely (**Fig. 2c**).

How many target molecules are collected as the depleted zone develops? Target molecules diffuse down concentration gradients with flux (molecules per area per time) $j_D = -D\nabla c$. For scaling purposes, the gradient ∇c can be simply estimated as the change in concentration (here $\Delta c = c_0$) divided by the distance δ over which it changes, so that $j_D \sim Dc_0/\delta$. As well, the total collection rate J_D (molecules/time) scales roughly like the target flux j_D multiplied by the area through which it proceeds. For times $t \ll L^2/D$, where the depletion zone is
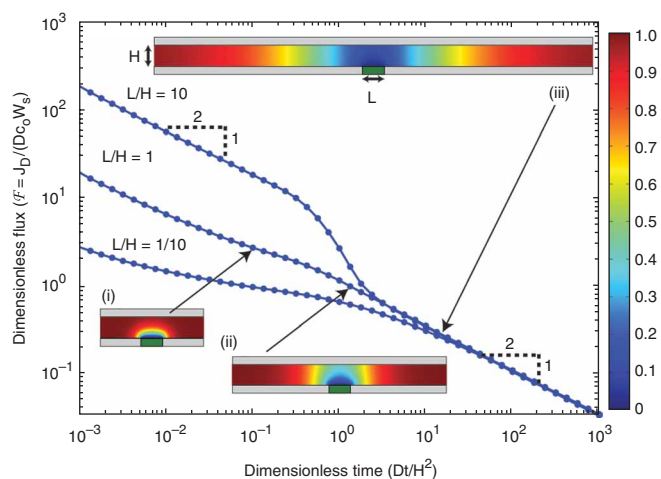
Figure 2 Purely diffusive flux to sensors of three different sizes ($\lambda = L/H$): $\lambda = 10$ (top), $\lambda = 1$ (middle), and $\lambda = 1/10$ (bottom), computed using COMSOL. We plot a dimensionless flux $\mathscr{F} = J_D/(Dc_0W_s)$ as a function of dimensionless time $\tilde{t} = Dt/H^2$, assuming for simplicity the sensor is as wide as the channel. Inset plots i–iii show the depletion zones for various relevant times for a sensor with $\lambda = 1$: (i) $t \ll L^2/D$, where the depletion zone is essentially planar; (ii) $t \sim H^2/D$, when it 'feels' the finite channel height, and (iii) t$\gg H^2/D$, where it extends far into the channels and is essentially uniform across the channel. At these long times, the collection flux $\mathscr{F}$ is independent of sensor size. Note that no steady state is ever reached.

basically planar, $J_D \sim (Dc_0/\delta)LW_s \sim LW_sc_0\sqrt{D/t}$. When the depletion zone extends into the channels, that is, for times $t \gg H^2/D$, the flux j_D proceeds along the channels (with cross-sectional area HW_c), giving a collection rate $J_D \sim (Dc_0/\delta)HW_c \sim HW_cc_0\sqrt{D/t}$ that is largely independent of the sensor size L.

To plot these results in a general way, we introduce scales for time and flux. Because τ_D represents a natural time scale in this system, we 'measure' time in units of τ_D. For example, a target protein with $D = 10$ μm^2/s takes $\tau_D \sim 10$ s to diffuse across a 10-μm channel. Similarly, a natural scale for the total flux J_D is Dc_0W_s. In **Figure 2**, a dimensionless flux function $\mathscr{F}$, defined by

$$\mathscr{F} = \frac{J_D}{Dc_0W_s} \qquad (1)$$

is plotted against dimensionless time $\tilde{t} = t/\tau_D = Dt/H^2$ for different dimensionless sensor lengths $\lambda = L/H$. In so doing, **Figure 2** is valid for any such system, irrespective of c_0 H, D, L or t. For example, at 'long' times (compared with τ_D), the (dimensionless) diffusive flux for all three sensor sizes collapses onto a single limiting curve with (log-log) slope $-1/2$, indicating $\mathscr{F} \sim \tilde{t}^{-1/2}$. This occurs when the depletion region is so long that it poses the major impediment to collection, as discussed above. To connect these dimensionless quantities back to real numbers for specific systems, one must simply compute the dimensional versions, that is, $J_D = Dc_0W_s\mathscr{F}$ and $t = H^2\tilde{t}/D$.

Before moving on to treat flow, we note a few things. First, steady state is never reached in these two-dimensional systems (which become effectively one-dimensional as depletion zones extend far into the channels). The depletion zone grows ever larger, diffusive flux gets ever smaller, and collection ever slower. Second, this result depends crucially on the dimension of the sensor: sensors whose size is limited in all three dimensions—for example, the depletion zones around spherical beads or microarray spots do reach a steady state, with sizes set roughly by the size of the

sensor. For example, the steady collection rate for a sphere of radius L is given by $J_D^s = 4\pi Dc_0L$ (ref. 29).

Going with the flow

Thus far, we have discussed purely diffusive transport—the random motion of target molecules through the surrounding fluid. We now add convective transport—the motion of target molecules along with a fluid flow with velocity,

$$u = \frac{6Q}{W_cH^3}z(H-z) \qquad (2)$$

which we assume to be pressure-driven Poiseuille flow with volumetric flow rate Q, and parabolic dependence on the height z above the sensor. This apparently simple addition complicates the mathematical solution tremendously, admitting exact solutions only in rare circumstances. The difficulty is that these systems often contain some regions where diffusion dominates, and others where convection dominates. Mathematically speaking, any approximation scheme that works in one region is bound to fail in the other. 'Matched asymptotic' techniques employ different approximations in different regions, and require them to 'match' seamlessly into each other. We use here the spirit (but not the detail) of matched and multi-scale asymptotics to arrive at intuitive and quantitative scaling relations, and refer the interested reader to graduate texts in transport[26,27] or asymptotics[23,24].

Fundamental, qualitative changes are seen when flow is introduced into our ideal sensor. Imagine now that we pump a target solution through the channel with an extremely slow rate Q. (The attentive reader should be asking, "slow compared to what?" We'll return to this shortly.) Recall that the purely diffusive depletion zone grows like $\delta \sim \sqrt{Dt}$ indefinitely into the channels, collecting target molecules ever more slowly (**Fig. 2c**). Convection halts this growth, giving a steady depletion zone with just the right length δ_s for the target flux delivered by convection ($J_C = c_0Q$, in molecules/s) to precisely balance the diffusive flux through the upstream depletion zone ($J_D \sim Dc_0HW_c/\delta_s$), giving $\delta_s \sim DHW_c/Q$ (**Fig. 3**). If the depletion zone $\delta(t)$ at some time is smaller than this steady value δ_s, the diffusive flux is too strong for convective flux to keep up, causing δ to grow and reign in diffusion. By contrast, if $\delta(t) > \delta_s$, diffusion cannot keep up convective delivery of target molecules, and the depletion zone is compressed. For slow enough flow rates, the sensor collects every target molecule that is injected, so that $J_D \approx Qc_0$.

So when is a flow 'extremely slow'? Diffusion always dominates close to the sensor, and convection always wins far away. However, the above picture requires diffusion to win over a region that extends substantially upstream: $\delta_s \sim DHW_c/Q$ must be much larger than the channel height H, limiting the flow rate to $Q \ll DW_c$. The same condition can be understood from a molecular standpoint. Does it take longer for a target molecule to diffuse across the channel (τ_D), or to be swept downstream (with average velocity Q/HW_c) that same distance? The ratio of these two time scales,

$$\frac{\text{diffusive time}}{\text{convective time}} \sim \frac{H^2/D}{H^2W_c/Q} \sim \frac{Q}{DW_c} \equiv \mathrm{Pe}_H \qquad (3)$$

is called the Peclet number[25–27], here with subscript H to specify the channel height as the relevant length scale. When $\mathrm{Pe}_H \ll 1$, diffusion wins, and a depletion zone does indeed propagate upstream a distance $\delta_s \sim H/\mathrm{Pe}_H$ (**Fig. 3c**). When $\mathrm{Pe}_H \gg 1$, on the other hand, the picture changes substantially (**Fig. 3d–i**).
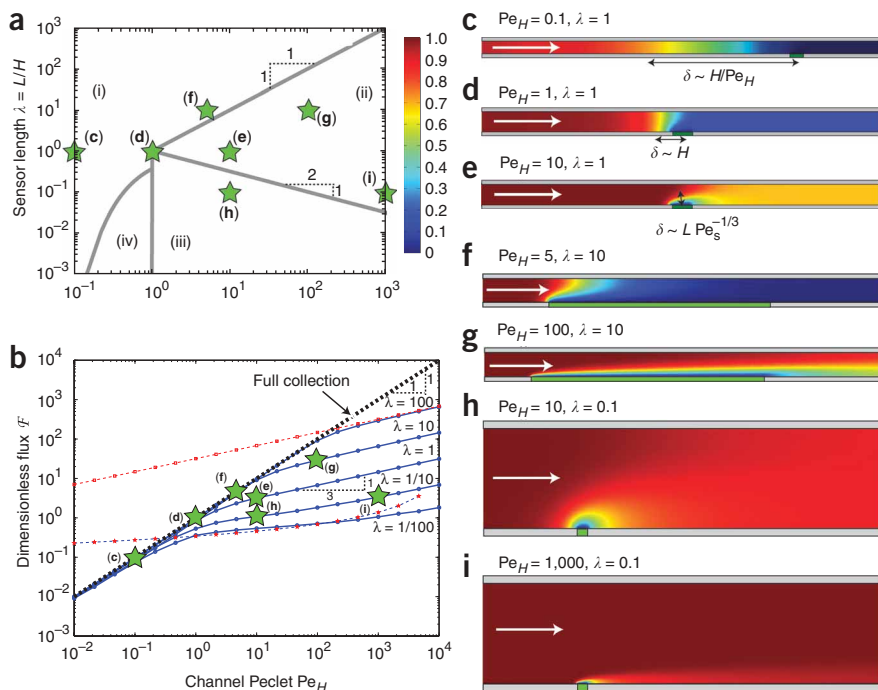
Figure 3 Mass transport and steady-state flux. (**a**) 'Phase diagram' for mass transport in our model sensing system. 'Full collection' occurs at sufficiently low Pe_H (and large enough sensor λ), corresponding to region i. In region ii, a depletion zone ($\delta_s \sim L Pe_s^{-1/3}$) forms that is thin compared to both the sensor length L and the channel height H, with collection flux given by equation 7 in main text. In region iii, the depletion zone ($\delta_s \sim L/Pe_s^{1/2}$) is thinner than the channel, but thicker than the sensor, with flux given by equation 8. Region iv has not, to our knowledge, been studied thus far. The boundaries between these regions are described in **Supplementary Notes**. (**b**) COMSOL computations of the total steady-state flux to the sensor under both convection and diffusion, plotted as a dimensionless quantity $\mathscr{F} = J_D/(Dc_0 W_s)$. Results are shown for a variety of sensor sizes $\lambda = L/H$, and compared with approximate formulas for full collection (black dashed line), thin depletion zone at $Pe_H \gg 1$ and $Pe_s \gg 1$ (red dashed line, from Newman[30]), $Pe_H \gg 1$, $Pe_s \ll 1$ (blue dashed line, from Ackerberg et al.[31]). (**c–i**) Steady concentration profiles are shown for different values of Pe_H and λ, corresponding to the stars in **a** and **b**. White arrows denote flow direction, and the sensor has the same width as the channel.

As above, we plot and report the collection flux in terms of a dimensionless flux function $\mathscr{F}$ from which the (dimensional) flux can be obtained via $J_D \approx Dc_0 W_s \mathscr{F}$. (In the mass-transport literature, this nondimensionalized flux is known as the Sherwood number.) With 'extremely slow' flows ($Pe_H \ll 1$), all target molecules are collected and $\mathscr{F} \sim Pe_H$ (**Fig. 3**).

So we turn to the opposite extreme of 'extremely fast' flows, where target molecules are swept downstream before they can diffuse very far, and the only target molecules that stand a chance of collection lie in a thin layer above the sensor. In this case, the relevant target molecules do not 'see' the full parabolic flow in the channel, but only the linear shear flow $u = \dot{\gamma}z$ at a height z above the sensor, where $\dot{\gamma} = 6Q/H^2 W_c$. How thick is the steady depletion zone δ_s in this case? Target molecules that flow a distance δ_s above the sensor (that is, right at the edge of the zone) require $\tau_c \sim L/(\dot{\gamma}\delta_s)$ to convect past the sensor. The 'thickness' of the depletion zone (in a scaling sense) is that value δ_s where the time τ_c to convect past the sensor is just enough for the target molecules to diffuse across the distance δ_s and be collected (that is, $\tau_c \sim \delta_s^2/D$). The depletion zone thus has thickness

$$\frac{\delta_s}{L} \sim \left(\frac{D}{\dot{\gamma}L^2}\right)^{1/3} \sim \left(\frac{DH^2 W_c}{QL^2}\right)^{1/3} \sim \left(\frac{1}{Pe_s}\right)^{1/3} \quad (4)$$

where

$$Pe_s = \frac{\dot{\gamma}L^2}{D} = 6\lambda^2 Pe_H \quad (5)$$

is a second Peclet number that depends upon shear rate and sensor length. Pe_s must be large for this picture to hold. The flux through the depletion zone can be estimated as

$$J_D \sim \frac{Dc_0}{\delta} W_s L, \text{ so } \mathscr{F} \sim Pe_s^{1/3} \quad (6)$$

as can be seen in **Figure 3** for large Pe_s. Newman[30] computed the full problem more accurately, obtaining

$$\mathscr{F}(Pe_s \gg 1) \approx 0.81 Pe_s^{1/3} + 0.71 Pe_s^{-1/6} - 0.2 Pe_s^{-1/3} \cdots \quad (7)$$

The total mass transport varies only weakly with flow rate in this limit: flow rates must be increased 1,000-fold to enhance flux by a factor of ten.

Two Peclet numbers, Pe_H and Pe_s, naturally emerge from this analysis. Each describes a distinct competition between convection and diffusion, and each says something qualitatively different about the depletion zone itself. The former describes the sensor's 'range of influence': the depletion zone extends far upstream if $Pe_H \ll 1$, but is thinner than the channel if $Pe_H \gg 1$. The second, Pe_s, indicates whether the depletion zone is thick or thin relative to the sensor itself.

This distinction is particularly important when the sensor and channel have different characteristic scales—for 'small' sensors ($L \ll H$, as with nanowires): the depletion zone can be thicker than the sensor, but thinner than the channel (that is, $Pe_H \gg 1$ but $Pe_s \ll 1$). Any convection prevents the depletion zone from growing indefinitely, giving a thickness that scales like $L/Pe_s^{1/2}$ and a collection flux

$$\mathscr{F} \approx \pi(\ln(4/Pe_s^{1/2}) + 1.06)^{-1} \quad (8)$$

that vanishes extremely slowly as $Pe_s \to 0$, as calculated by Ackerberg et al.[31]. This treatment assumes the depletion zone to be nearly two-dimensional, which will generally work so long as the sensor is much wider than the depletion zone is thick ($W_s \gg L/Pe_s^{1/2}$). The above formulae also hold for microarray pixels (where $W_s \sim L$) so long as $Pe_s \gg 1$. When $Pe_s \ll 1$, however, the third dimension matters and disks become more appropriate models than strips. Approximate low-Pe_s[31] and high-Pe_s[30] formulae for mass transport to strips and disks under shear flow are treated and discussed by Zhang et al.[32]. A 'phase diagram' showing the qualitatively different depletion zones, and their corresponding collection fluxes, is shown in **Figure 3**. We saw above that at sufficiently low Pe_H, all target molecules that enter the channel are collected by the sensor. A plot of this 'retained' fraction for various Pe_H and λ appears as **Supplementary Figure 2** online.

Having treated both convection and diffusion, one can now simply compute the dimensionless numbers Pe_s and Pe_H to determine

Box 1 Example microscale and nanowire sensors

We first consider a microscale sensor, modeled as a flat square of width $L = 50$ μm and length $W_s = 50$ μm, in a microchannel of height $H = 100$ μm and width $W_c = 100$ μm, through which a solution of target protein with concentration $c_0 = 10$ fM and diffusivity $D = 10$ μm²/s flows with rate $Q = 10$ μl/min. First-order reaction kinetics are assumed with $k_{on} = 10^6$ M⁻¹ s⁻¹ and $k_{on} = 10^{-3}$ s⁻¹, giving $K_D = 1$ nM, and binding-site density is assumed to be optimized at $b_m = 2 \times 10^{12}$ sites/cm².

Mass transport: convection and diffusion limits. The channel Peclet number, $Pe_H = Q/W_cD = 1.7 \times 10^5$, indicates that the depletion zone is much thinner than the channel. Using $\lambda = L/H = 0.5$, the shear Peclet number is $Pe_s = 6\lambda^2Pe_H = 2.5 \times 10^5$. The large value of Pe_s indicates that the depletion zone is much thinner than the sensor—$\delta_s \sim L_s/Pe_s^{1/3} \sim 800$ nm. The (dimensionless) mass-transport flux is then given by equation 7 to be $\mathcal{F} \approx 50$. In dimensional terms, $J_D = Dc_0W_s\mathcal{F} = 0.15$ molecules per second, or one molecule every 6 to 7 s. This represents an upper limit imposed on analyte collection by mass transport, which may be further lowered by finite reaction kinetics.

Reaction limits. The dimensionless concentration $\tilde{c} = c_0/K_D = 10^{-5}$ is very low, indicating that only a small fraction $b_{eq}/b_m = \tilde{c}/(1+\tilde{c}) \approx 10^{-5}$ of the available sites will actually be bound in equilibrium. Because there are $N_R = b_mW_sL = 5 \times 10^7$ total binding sites, the concentration at which approximately one molecule will be bound to the sensor in equilibrium is given by $c^* = K_D/N_R \approx 20$ a.m., which is 500 times lower than c_0. We thus expect an average number $N_R^B = N_Rc_0/K_D = 500$ target molecules to be bound in equilibrium, irrespective of how the system reaches equilibrium.

The Damkohler number indicates how equilibrium is reached: because $Da = k_{on}b_mL/D\mathcal{F} \approx 3$ is neither large nor small, the microsensor operates neither in the reaction-limited nor diffusion-limited regime. The time to equilibrate the sensor can be read approximately from **Figure 5**: at $Da \approx 3$, the time scale for equilibration τ_{CRD} is around three to four times the reaction time scale τ_R $\tau_R \sim k_{off}^{-1}$ or ~ 1 h (**Fig. 4** (left)).

Next, we consider a nanowire sensor, modeled as a flat strip of length $L = 10$ nm and width $W_s = 2$ μm. All other parameters are the same as for the microsensor (**Fig. 4** (right)).

Mass transport: convection and diffusion limits. As with the microsensor, the channel Peclet number, $Pe_H = 1.7 \times 10^5$, indicates that the depletion zone is much thinner than the channel. The smaller sensor gives $\lambda = 10^{-4}$ and $Pe_s = 10^{-2}$, indicating that the depletion zone is thicker than the sensor ($\delta_s \sim L_s/Pe_s^{1/2} \approx 100$ nm) and that the (dimensionless) mass-transport flux $\mathcal{F} \approx 0.7$ is given by equation 8 from the main text. In dimensional terms, $J_D = Dc_0W_s\mathcal{F} = 8 \times 10^{-5}$ molecules bind per second, or one molecule every 210 min. Again, this represents an upper limit for collection imposed by mass transport alone.

Reaction limits. As for the microsensor, a small fraction $b_{eq}/b_m \approx 10^{-5}$ of the available sites will actually be bound in equilibrium. Given that there are $N_R = b_mW_sL = 400$ total binding sites, $c^* = K_D/N_R \approx 2.5$ pM. Because the target concentration $c_0 = 10$ fM is much smaller than c^*, we expect the sensor to be essentially 'empty', even in equilibrium. In fact, the equilibrium number of bound molecules is $N_R^B = N_Rc_0/K_D = 0.004$: the sensor will be bound to a single target molecule <1% of the time. Again, these values hold irrespective of the kinetic approach to equilibrium.

As for kinetics, the nanowire sensor is reaction limited because $Da = k_{on}b_mL/D\mathcal{F} = 0.03$. Mass transport is thus essentially instantaneous, and binding proceeds exponentially with time constant $k_{off}^{-1} \approx 17$ min. Actual experiments with individual nanowires would look nothing like the Langmuir binding curve (equation 10 in main text), however. Assuming single-binding events could be clearly resolved experimentally, nothing would be bound 99.6% of the time, with one target molecule bound 0.4% of the time. On average, each measured binding event would last $k_{off}^{-1} \approx 17$ min, suggesting ~ 17 min/.004 ≈ 3 days between binding events. One thousand nanowire experiments, run in parallel, would yield a total of four bound target molecules, on average, at any given time.
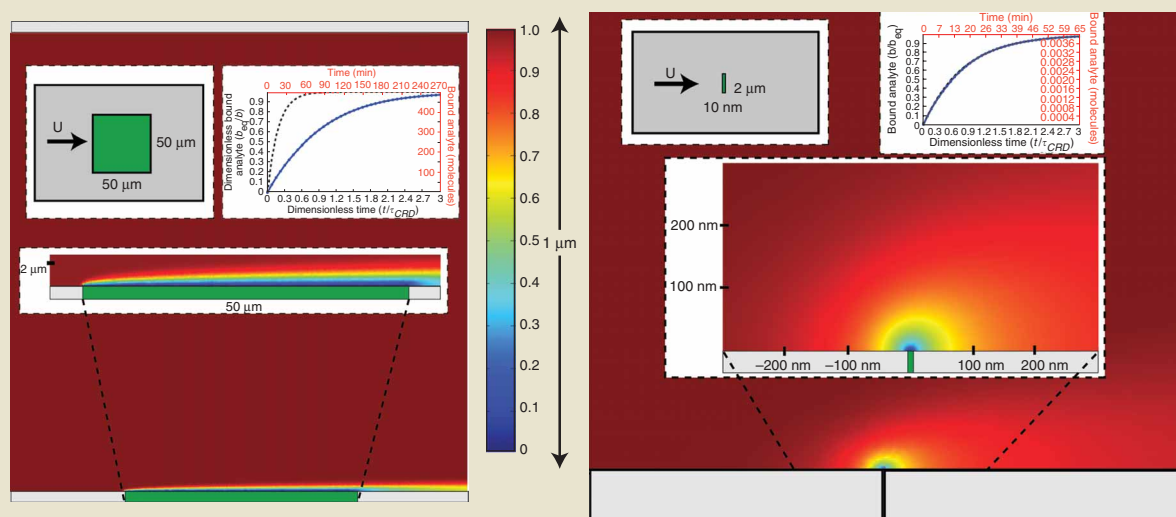

Figure 4 Example sensors: a microscale sensor (left) and a nanowire sensor (right). Shown are the steady-state depletion zone from the pure mass-transport problem; both have very high Pe_H so that the depletion zone is substantially thinner than the channel itself. The depletion zone is thin compared to the microsensor (from equation 4, $\delta_s \sim 800$ nm) and thick compared to the nanowire ($\delta_s \sim LPe_s^{-1/2} = 100$nm), as can be seen in the inset figures. Reaction-limited binding onto the nanowire follows the Langmuir binding curve (inset, right) whereas the $Da \approx 3$ binding for the microsensor is neither reaction nor diffusion limited, yielding an equilibrated sensor on a time scale three to four times longer than the reaction-limited time scale.

the mass-transport regime in which a given device operates (or, conversely, how to design a device to operate within a desired regime). **Box 1** and **Figure 4** illustrate two example sensors with very different length scales: a nanowire and a microsensor (e.g., an optical microcavity or protein microarray pixel). The channel Peclet for protein targets is large for both devices ($Pe_H = 1.7 \times 10^5$), yielding depletion zones that are substantially thinner than the channel. The sensor Peclet, however, differs for the two devices: $Pe_s = 2.5 \times 10^{-2}$ for the nanowire, whereas $Pe_s = 2.5 \times 10^5$ for the microsensor. The depletion zone is thus larger than the nanowire, but thinner than the microsensor. The collection rate is given by equation 8 for the nanowire, and by equation 7 for the microsensor. For target concentrations of 10 fM, the interval between binding events is ~ 3 h for the nanowire—substantially longer than experimental results, where saturation (not just single events) has been reported to occur in seconds to minutes[17,18]. Under similar conditions, the microsensor requires 7-s intervals between binding events at 10 fM. This time scales inversely with concentration—optical microcavities with somewhat smaller active sensing surfaces have detected binding intervals of a few seconds[19] in 100 aM solutions, whereas ~ 10 min would be expected from theory. A tenfold increase in flow rate reduces these intervals by $\sim 25\%$ for the nanowire and 50% for the microsensor, insufficient to account for the many order-of-magnitude discrepancies between measured values and the mass-transport limits for both nano- and microscale sensors. These discrepancies suggest that other factors must be accelerating the binding, a topic to which we return below.

Making it stick

One final hurdle remains before target molecules bind and are sensed: the chemical reaction itself. Assuming first-order Langmuir kinetics for simplicity, the surface concentration $b(t)$ of receptors that are bound by target molecules obeys

$$\frac{\partial b}{\partial t} = k_{on}c_s(b_m - b) - k_{off}b, \qquad (9)$$

where b_m is the surface concentration of receptors on the sensor. Binding depends on the concentration of unbound sites ($b_m - b$) and on target concentration c_s at the sensor surface, whereas target molecules de-bind in proportion to the bound concentration. If convective and diffusive transport supply target molecules much more quickly than reactions can bind them, then transport is 'reaction limited', $c_s \approx c_0$ and equation 9 can readily be solved:

$$\frac{b(t)}{b_m} = \frac{c_0/K_D}{1 + c_0/K_D}\left(1 - e^{-(k_{on}c_0 + k_{off})t}\right), \qquad (10)$$

where the equilibrium dissociation constant $K_D = k_{on}/k_{off}$ appears as a natural concentration scale. Although this is probably familiar to one trained in physical chemistry, we focus on a few key features here for emphasis.

First, the fraction of bound receptors in equilibrium, b_{eq}, is given by

$$\frac{b_{eq}}{b_m} = \frac{c_0/K_D}{1 + c_0/K_D} \equiv \frac{\tilde{c}}{1 + \tilde{c}} \qquad (11)$$

irrespective of how long the sensor takes to equilibrate. Here $\tilde{c} = c_0/K_D$ is the concentration, nondimensionalized by the natural concentration scale K_D. Concentrated solutions ($\tilde{c} \gg 1$, or equivalently $c_0 \gg K_D$) effectively saturate the sensor, whereas dilute solutions ($\tilde{c} \ll 1$) bind only a fraction $b_{eq} \sim c_0b_m/K_D \ll b_m$. Serious consequences can result for small sensors and dilute

solutions: a sensor with area A has $N_R = b_mA$ receptors, of which the number N_R^B that are bound in equilibrium is given by $N_R^B \sim b_mA\tilde{c} = b_mAc_0/K_D$. This naturally gives rise to a critical concentration,

$$c^* = \frac{K_D}{b_mA} \qquad (12)$$

at which only one target molecule binds the sensor in equilibrium. Less concentrated solutions ($c_0 < c^*$) yield a fraction of a target molecule bound at equilibrium. This seemingly unphysical result reflects the ensemble average that underlies this approach, and simply indicates that a target molecule will be bound to the sensor only this fraction of the time (or only in this fraction of the experiments at any given time). Solutions that are not appreciably more concentrated than c^*, therefore, will inherently involve noisy, time-fluctuating single-molecule binding and debinding events.

For example, assuming an antibody binding affinity $K_D = 1$ nM, c^* can be estimated for sensors of various sizes. The density of active binding sites, b_m, depends strongly on the immobilization procedure, and extensive effort has been directed toward optimizing binding efficiency[33]. If only the antigen-binding portion of the antibody is isolated and attached to the surface such that it is well oriented, a near monolayer can be created with an active site density as high as $b_m = 2 \times 10^{12}/\text{cm}^2$. If, however, the entire antibody is used and randomly attached to the surface (thereby blocking many of the active sites), b_m is reduced by an order of magnitude or more. Assuming b_m to be optimized, a single 2 µm × 10 nm hemicylindrical nanowire has $N_R \sim 10^3$ binding sites, giving $c^* \sim 10^{-3}$ and $K_D \sim 1$ pM. Target detection in more dilute solutions would require one to resolve single-molecule binding events. By contrast, a 50 µm × 50 µm microsensor has $\sim 5 \times 10^7$ binding sites and thus $c^* \sim 20$ a.m. is much lower.

The other key point from equation 10 involves the time scale

$$\tau_R = (k_{off} + k_{on}c_0)^{-1} = k_{off}^{-1}(1 + \tilde{c})^{-1} \qquad (13)$$

required for the sensor to equilibrate in the reaction-limited case. At high concentrations ($\tilde{c} \gg 1$, or $c_0 \gg K_D$), nearly all sites must be bound ($b_{eq} \sim b_m$), so that the equilibration time reflects how long the 'on' kinetics take to deliver sufficient target molecules. At low concentrations ($\tilde{c} \ll 1$, or $c_0 \ll K_D$), however, relatively few sites are bound in equilibrium ($b_{eq} \ll b_m$), and steady state is not achieved by binding this many target molecules. Rather, equilibration requires the on and off fluxes to balance, which effectively requires that those target molecules that do bind have sufficient time to unbind. The equilibration time for dilute solutions is thus determined solely by the off rate: $\tau_R \sim k_{off}^{-1}$.

Bringing it all together

We have now encountered two independent 'speed limits' for target collection. The mass-transport limit occurs when convection and diffusion deliver target molecules so slowly that the time for the reaction itself is negligible by comparison. This collection rate is $J_D \sim Dc_0W_s\mathscr{F}$, where $\mathscr{F}$ can be read off of **Figure 3** so long as Pe_H and λ are known. The reaction itself provides the other limit, when mass transport would be much faster by comparison; in this case the initial reactive flux is $J_R \sim k_{on}b_mc_0LW_s$. Collection rates can never exceed either of these limits. In general, reaction kinetics are determined by the fidelity of the immobilized
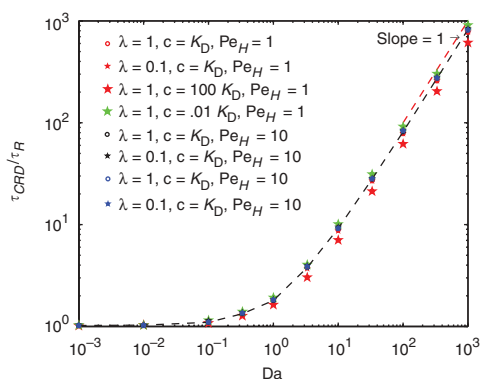
Figure 5 The equilibration time τ_{CRD}, normalized by the reaction time τ_R, plotted as a function of the Damkohler number Da, as in equation 20 in the main text. When Da $\ll$ 1, $\tau_{CRD} \sim \tau_R$, as mass transport is essentially irrelevant. When Da $\gg$ 1, convection and diffusion are rate limiting, extending the equilibration time to $\tau_{CRD} \sim \mathrm{Da}\tau_R$. Notably, a wide range of concentrations and flow rates collapse onto a single, master curve. Here we have chosen $\varepsilon \ll 1$ in order that the quasi-steady approximation holds; otherwise, τ_{CRD} for 'unsteady' systems would be shorter.

reagents; and sensor size and flow rate can be more easily adjusted to aim for the reaction-limited regime.

When is the reaction limit achieved? With the intuition developed above, we now turn to the full convection-diffusion-reaction system, and address the kinetic approach to equilibrium.

To illustrate, we start with the $\mathrm{Pe}_s \gg 1$ limit, where a thin depletion zone forms above the sensor. Here, though, the concentration c_s at the sensor surface (which is as yet unspecified) regulates the two fluxes, as seen below. Diffusion cares only about gradients, not absolute concentration, so that the mass-transport arguments developed above still hold, with $(c_s - c_0)$ in place of c_0. The mass-transport flux through the boundary layer is thus

$$J_D \sim \frac{D(c_0 - c_s)L}{\delta}W_s, \qquad (14)$$

and the (initial) reactive flux is

$$J_R \sim k_{on}c_s b_m L W_s \qquad (15)$$

Assuming binding occurs quasi-steadily (as discussed shortly), diffusive flux through the depletion zone must balance the reactive flux onto the sensor. This balance ($J_R = J_D$) gives an expression for the concentration at the surface,

$$\frac{c_s}{c_0} \sim \frac{1}{1 + k_{on}b_m\delta/D} = \frac{1}{1 + \mathrm{Da}}, \qquad (16)$$

wherein the Damkohler number, $\mathrm{Da} = k_{on}b_m\delta/D$ is a ratio of reactive to diffusive flux. If Da $\gg$ 1, mass transport is rate limiting—correspondingly, c_s is nearly zero to slow the reaction. If Da $\ll$ 1, on the other hand, then reactions are slow enough to restrain an otherwise fast diffusive flux; the latter is slowed because $c_s \sim c_0$ and concentration gradients are weak. This analysis corresponds directly to the two-compartment model widely used to interpret SPR experiments, wherein c_s and c_0 are interpreted as 'inner' and 'outer' compartments, between which molecules transport with the $\mathrm{Pe}_s^{1/3}$ scaling characteristic of thin boundary layers[34].

More generally, one can compute the surface concentration in the quasi-steady limit by equating the reactive flux $J_R \sim k_{on}c_s b_m L W_s$

with the mass-transport flux $J_D \sim D(c_0 - c_s)W_s\mathscr{F}$, yielding

$$\frac{c_s}{c_0} \sim \left(1 + \frac{k_{on}b_m L}{D\mathscr{F}}\right)^{-1}, \qquad (17)$$

and a general Damkohler number

$$\mathrm{Da} = \frac{k_{on}b_m L}{D\mathscr{F}} \qquad (18)$$

As before, kinetics are reaction limited if Da $\ll$ 1 and mass transport−limited if Da $\gg$ 1. In the reaction-limited regime, mass transport is largely irrelevant, and binding equilibrates on a time scale τ_R (equation 13).

How long will equilibration take when Da $\gg$ 1, when mass transport through the bulk solution is rate limiting? The diffusive flux is given by

$$j_D \sim \frac{D(c_0 - c_s)\mathscr{F}}{L} \sim \frac{Dc_0\mathscr{F}}{L}, \qquad (19)$$

since $c_s \ll c_0$ in diffusion-limited systems. Note that j_D will not depend appreciably upon c_s or b so long as the system remains diffusion limited. Once the bound receptor concentration b starts to approach its equilibrium concentration $b_{eq} = b_m\tilde{c}/(1 + \tilde{c})$, surface reactions will slow, c_s will increase, and the system will leave the diffusion-limited regime. However, j_D remains nearly constant until b/b_{eq} becomes appreciable, which is when sensor saturation begins to occur. The equilibration time in the convection-reaction-diffusion system, τ_{CRD}, is given in the diffusion-limited case by

$$\tau_{CRD}(\mathrm{Da} \gg 1) \sim \frac{b_{eq}}{j_D} \sim \frac{k_{on}b_m L}{D\mathscr{F}(k_{off} + k_{on}c_0)} = \mathrm{Da}\tau_R, \qquad (20)$$

and thus exceeds the reaction-limited time scale by a factor Da. Example simulations showing how the bound concentration grows in a reaction-limited system and a diffusion-limited system appear in **Supplementary Figure 3** online. **Figure 5** plots equilibration time τ_{CRD} against Da for a range of flow rates and conditions, for which τ_{CRD} would vary by orders of magnitude if unscaled. Suitably scaling τ_{CRD} by τ_R and plotting against Da, however, collapses this extraordinary range of conditions to lie upon a single, universal curve. Reaction-limited systems (Da $\ll$ 1) equilibrate on the reaction time scale τ_R, and diffusion-limited systems (Da $\gg$ 1) equilibrate on a longer time Daτ_R.

To examine the effects of finite reaction kinetics upon example micro- and nanosensors, we turn to **Box 1**. For typical flow rates and kinetic parameters, nanowire sensors are reaction limited (Da $\sim$ 0.04) and equilibrate on time scales $\tau_{CRD} \sim k_{off}^{-1} \sim$ 17 min for low target concentration. This may seem at first to exceed the mass-transport limit of 3 h between binding events in 10-fM solution. Recall, however, that $c^* = 2.5$ pM for the nanowire; as such, an unphysical '4×10^{-3} target molecules' binds to the nanowire in equilibrium in 10-fM solution. A more sensible interpretation is that a single nanowire will bind a single target molecule $\sim$0.4% of the time, or that 1,000 independent nanowire sensors will, on average, find four target molecules bound at any given time. Because each binding event lasts, on average, 17 min, one expects $\sim$3 days between binding events. Our example microsensors, on the other hand, have Da $\approx$ 3 and thus operate strongly in neither limit. SPR devices, as well, may operate in either the mass-transport limited or reaction-limited regimes[34].

Coping with change

We have assumed that the sensor equilibrates slowly enough that the depletion zone evolves 'quasi-steadily'—that is, mass transport is given by the steady-state flux $\mathscr{F}$. The two-compartment model for SPR devices makes a similar assumption[34]. When is it valid? The time scale for the reactive flux to change appreciably (that is, τ_{CRD}) must be much greater than the time scale for the depletion zone to form ($\tau_\delta \sim \delta_s^2/D$, where $\delta_s \sim Pe_s^{-1/3}L$ for $Pe_s \gg 1$, $\delta_s \sim Pe_s^{-1/2}L$ for $Pe_s \ll 1$ and $Pe_H \gg 1$, and $\delta_s \sim H/Pe_H$ for $Pe_H \ll 1$). Requiring $\tau_\delta \ll \tau_{CRD}$ gives

$$\varepsilon = \frac{\tau_\delta}{\tau_{CRD}} = \frac{K_D(1+\tilde{c})\delta^2 \mathscr{F}}{b_m L} \ll 1. \qquad (21)$$

This ratio ε may be obtained in a different fashion as well. The number of target molecules collected as the depletion zone is formed (that is, $V_\delta c_0$, where V_δ is the volume of the depletion zone around the sensor) must be substantially fewer than the number required to saturate the sensor $N_R \sim b_{eq}LW_s \sim b_m c_0 LW_s/(K_D + c_0)$. All of our computations have been run in the quasi-steady limit, although one can certainly find systems where this limit is not appropriate.

So where are we? We have painted a fairly comprehensive picture of a model biosensing system that accounts for convection, reaction and diffusion in an intuitive manner, from which we have derived accurate, order-of-magnitude scaling relations for fluxes and time scales. For biosensor development, knowing the 'speed limits' can be helpful for interpreting data. If binding events are measured to be faster than these limits, then other transport mechanisms must be occurring.

Breaking the limits

Situations where the speed limits we've discussed thus far are violated are not without precedent in other systems. Electrostatic interactions between charged molecules and oppositely charged surfaces or receptor molecules can accelerate binding, particularly at low ionic strengths where 'screening lengths' are large[35]. For example, the association rate constant k_{on} for the specific interaction of colicin nucleases with their cognate immunity proteins have been shown to be enhanced by more than 100-fold in buffers containing low salt concentrations[36]. When the salt concentration is increased, electrostatic interactions are largely screened and the on-rate returns to the diffusion limit[37]. The response time of DNA microarrays can also be enhanced under certain conditions: under low salt concentration and in low pH where the surface is positively charged, DNA hybridization rates of 1-nM target concentration can be increased 80-fold[38]. Although electrostatic interactions can increase k_{on} and thereby decrease the critical concentration c^* at which one molecule is bound, the diffusion limit is hardly changed. Even so, applying electric currents can indeed alter mass transport to and from a surface[39].

Other mechanisms besides electrostatics can enhance binding. A striking example is the observation that the DNA binding protein, LacI repressor, finds its target sequence at rates much faster than the three-dimensional diffusion limit[40]. Clever single-molecule experiments[41] and theory[42] have shown that an enhancement of nearly 100-fold is due to a combination of one- and three-dimensional diffusion that the protein performs in a near-optimal fashion.

Alternatively, mass transport can be accelerated by actively decreasing the depletion zone thickness. Strategies explored include 'stirring' the depletion zone using various mixing strategies[43,44] and using a waste channel to withdraw the depletion layer and thus bring fully concentrated target solution to sensors downstream[43].

Box 2 Optimizing an HIV viral load measurement by surface capture

Here we use the analysis to design a hypothetical sensor that measures viral load for HIV by directly capturing virions to the sensor surface, thereby eliminating the need for PCR. We will consider the sensor to lie along the entire length of the channel and will generally assume the bound molecules are enumerated by any of the above-discussed methods (e.g., fluorescence, mass or charge). By applying a pressure $P = 100$ p.s.i. (e.g., limited by mechanical failure of the device), we drive a sample volume $V = 10$ ml containing a threshold concentration for HIV, $c = 10$ virions/μl (for 10^5 total virions) through a microchannel sensor of height H, width $W_c = 100$ μm, and length $L = 10$ mm. The goal is to choose a channel height that will allow a sufficient number of virions to be captured and sensed, and thus to measure viral load as quickly as possible. For simplicity, we will assume that virions are instantly captured upon encountering the surface and remain bound indefinitely (that is, diffusion limited).

The pressure-driven volumetric flow through the channel is given by

$$Q = \frac{H^3 W_c}{12\eta L}P, \qquad (22)$$

where η is the fluid viscosity (1 cP for water at room temperature). With this flow rate, a time

$$T = \frac{V}{Q} = \frac{12\eta LV}{H^3 W_c P}, \qquad (23)$$

is required to drive the entire sample volume through the channel. The mass transport is dictated by the channel and sensor Peclet numbers (equations 3 and 5)

$$Pe_H = \frac{H^3 P}{12\eta LD} \text{ and } Pe_s = \frac{HLP}{2\eta D}, \qquad (24)$$

where $D \approx 5$ μm²/s is the diffusivity of a 50-nm radius virion in water. To collect all virions during the measurement (e.g., region i in **Fig. 3a**), the depletion zone must be thicker than the channel height, $LPe_s^{-1/3} \gg H$, or $Pe_H \ll \lambda$, thus requiring

$$H \ll \left(\frac{12\eta L^2 D}{P}\right)^{1/4} \approx 1.7\,\mu m \qquad (25)$$

Indeed, all virions would be captured with a 1-μm tall channel; however, ~200 days would be required to complete the experiment! Taller channels enable faster flows and quicker measurements, but reduce the relative fraction of virions collected (which is given by the ratio of collection flux to input flux, $Pe_s^{1/3}/Pe_H$). The relative collection rate for a 10-μm channel is 0.017, such that 1.7% of the virions in the sample (that is, 1,700 virions) will be collected, in an experiment that takes ~5 h. A 100-μm channel, on the other hand, requires <20 s for the measurement, but will yield only four virions collected in total. It is evident that viral collection and measurement times depend quite strongly upon channel height. The optimal channel height for a specific experiment, then, will depend sensitively upon how many virons must be captured to be reliably measured over the noise specific to the sensor and also upon constraints on total measurement time.

Summary and conclusions

Throughout this article, we have explored sensor binding kinetics by thinking in extremes. Using dimensionless ratios to indicate the relative importance of competing effects, we have examined systems with large or small values of these dimensionless parameters to

develop intuition for qualitative behavior, and scaling relations for quantitative understanding. These dimensionless parameters are straightforward to compute, and are enormously useful in characterizing and designing systems. Two Peclet numbers characterize the nature of the mass-transport depletion zone around the sensor. The first, Pe_H, indicates the sensor's range of influence: the depletion zone is thin compared to the channel if $Pe_H \gg 1$, whereas it extends far upstream if $Pe_H \ll 1$. The second, Pe_s, is relevant when $Pe_H \gg 1$ and indicates whether the depletion zone is thick or thin relative to the sensor itself. These two parameters give rise to a (dimensionless) flux $\mathscr{F}$, plotted in **Figure 3**, from which the diffusion-limited collection rate can be computed by $J_D = D c_0 W_s \mathscr{F}$.

Chemical reaction kinetics gave rise to additional dimensionless parameters and natural concentration scales. A sensor's dynamic range is effectively bounded from below by c^*—the target concentration below which less than one molecule on average will be bound in equilibrium—and from above by K_D, above which the sensor is effectively saturated. How quickly the sensor equilibrates depends upon the dimensionless parameter Da (which itself depends upon mass-transport flux $\mathscr{F}$): if $Da \gg 1$, then equilibration is limited by the rate of target diffusion to the sensor, whereas the reaction itself limits sensor kinetics if $Da \ll 1$. Finally, ε indicates whether the quasi-steady approximation used throughout our presentation is valid—that is, whether the sensor equilibrates before the depletion zone has a chance to form.

How can researchers use this information in examining real biosensing systems? First and foremost, simply computing the above dimensionless parameters will give a good sense for how a given system behaves. Knowing the qualitative behavior regime enables one to know which approximations are appropriate, and thus to compute desired quantities using the scaling relations and figures here. The dimensionless formulae presented here are generally applicable. One must then 'put the units back in' to obtain reliable estimates for, for example, time scales and collection rates in a specific system. This approach will generally not help one to know whether 20 or 40 s will be required for sensor equilibration, but will confidently tell whether to expect 20 s or 20 min. In particular, such estimates are useful for determining whether or not a given measurement breaks the classic speed limit. Here, we have highlighted three reports in the literature where convection-reaction-diffusion theory predicted binding times that were two or more orders of magnitude longer than the measured response. Such discrepancies suggest that additional, as yet undetermined ingredients (beyond what we have incorporated here) must be present in the experiments. Numerical computations using more detailed experimental parameters will be required for more accurate predictions; whereupon the qualitative understanding developed here will help the interested researcher to choose appropriate numerical strategies.

Second, the above analysis will be useful in designing new sensors. No one sensor has emerged as optimal, or likely will, given the diversity in sensing mechanisms and their intended applications. Rather, optimizing sensor design requires collection performance (as defined for a particular objective) to be maximized subject to various constraints. The above analysis elucidates the design constraints imposed by transport. In some applications, sample volume is not a limiting factor (for example, in blood or saliva analysis), and 'designing' the transport to be reaction limited ($Da \ll 1$) will yield measurements as quickly as chemistry will allow. On the other hand, sensing in integrated microdevices may involve very small sample volumes, necessitating 'full collection' of the few target molecules present in the sample (region i, **Fig. 3a**). **Box 2** gives an optimization example. For all cases, one must ensure the sensor has

enough sites for target molecules to actually bind—that is, so that $c > c^*$ in equation 12—but also be mindful of signal/noise issues specific to the sensor.

As a final note, these systems are extraordinarily rich, and there is no way to cover all possibilities—even superficially—in a single article. For example, Gervais and Jensen[45] describe a convection-limited regime in their comprehensive treatment of microchannel sensors with $L \gg H$. When $c_0 H \ll b_m$ (that is, more binding sites on the wall than target molecules in the channel above it, per unit area) and when Da is high, target molecules only 'survive' in solution until they reach an unbound section of the sensor, establishing a traveling wave of equilibration.

We have attempted to treat the most common parameter regimes for surface-based sensors, and hope that this work will serve as a resource for many sensing systems. More broadly, however, we hope to have conveyed an intuitive style of thinking about target transport in these mathematically complex systems, thus enabling researchers to more rationally conceptualize, understand, control and design new sensing and reacting systems.

Note: Supplementary information is available on the Nature Biotechnology website.

1. The chipping forecast. *Nat. Genet.* **21**, S1 (1999).
2. The chipping forecast II. *Nat. Genet.* **32**, S4 (2002).
3. Johnsson, B., Lofas, S. & Lindquist, G. Immobilization of proteins to a carboxymethyl-dextran-modified gold surface for biospecific interaction analysis in surface-plasmon resonance sensors. *Anal. Biochem.* **198**, 268–277 (1991).
4. Rich, R.L. & Myszka, D.G. Survey of the year 2001 commercial optical biosensor literature. *J. Mol. Recognit.* **15**, 352–376 (2002).
5. Morgan, C.L., Newman, D.J. & Price, C.P. Immunosensors: technology and opportunities in laboratory medicine. *Clin. Chem.* **42**, 193–209 (1996).
6. Kartalov, E.P. et al. High-throughput multi-antigen microfluidic fluorescence immunoassays. *Biotechniques* **40**, 85–90 (2006).
7. Fritz, J. et al. Translating biomolecular recognition into nanomechanics. *Science* **288**, 316–318 (2000).
8. Wu, G. et al. Bioassay of prostate-specific antigen (PSA) using microcantilevers. *Nat. Biotechnol.* **19**, 856–860 (2001).
9. Bergveld, P. Development, operation, and application of ion-sensitive field-effect transistor as a tool for electrophysiology. *IEEE Trans. Biomed. Eng.* **BM19**, 342 (1972).
10. Souteyrand, E. et al. Direct detection of the hybridization of synthetic homo-oligomer DNA sequences by field effect. *J. Phys. Chem. B* **101**, 2980–2985 (1997).
11. Milovic, N.M. et al. Monitoring of heparin and its low-molecular-weight analogs by silicon field effect. *Proc. Natl. Acad. Sci. USA* **103**, 13374–13379 (2006).
12. Wang, J. Towards genoelectronics: electrochemical biosensing of DNA hybridization. *Chem. Eur. J.* **5**, 1681–1685 (1999).
13. Xiao, Y., Lubin, A.A., Baker, B.R., Plaxco, K.W. & Heeger, A.J. Single-step electronic detection of femtomolar DNA by target-induced strand displacement in an electrode-bound duplex. *Proc. Natl. Acad. Sci. USA* **103**, 16677–16680 (2006).
14. Burg, T.P. et al. Weighing of biomolecules, single cells and single nanoparticles in fluid. *Nature* **446**, 1066–1069 (2007).
15. Cui, Y., Wei, Q.Q., Park, H.K. & Lieber, C.M. Nanowire nanosensors for highly sensitive and selective detection of biological and chemical species. *Science* **293**, 1289–1292 (2001).
16. Bunimovich, Y.L. et al. Quantitative real-time measurements of DNA hybridization with alkylated nonoxidized silicon nanowires in electrolyte solution. *J. Am. Chem. Soc.* **128**, 16323–16331 (2006).
17. Zheng, G., Patolsky, F., Cui, Y., Wang, W.U. & Lieber, C.M. Multiplexed electrical detection of cancer markers with nanowire sensor arrays. *Nat. Biotechnol.* **23**, 1294–1301 (2005).
18. Stern, E. et al. Label-free immunodetection with CMOS-compatible semiconducting nanowires. *Nature* **445**, 519–522 (2007).

19. Armani, A.M., Kulkarni, R.P., Fraser, S.E., Flagan, R.C. & Vahala, K.J. Label-free, single-molecule detection with optical microcavities. *Science* **317**, 783–787 (2007).

20. Benn, J.A. *et al.* Comparative modeling and analysis of microfluidic and conventional DNA microarrays. *Anal. Biochem.* **348**, 284–293 (2006).

21. Melin, J. & Quake, S.R. Microfluidic large-scale integration: the evolution of design rules for biological automation. *Annu. Rev. Biophys. Biomol. Struct.* **36**, 213–231 (2007).

22. Sheehan, P.E. & Whitman, L.J. Detection limits for nanoscale biosensors. *Nano Lett.* **5**, 803–807 (2005).

23. Bender, C.M. & Orszag, S.A. *Advanced Mathematical Methods for Scientists and Engineers* (McGraw Hill, New York, 1978).

24. Hinch, E.J. *Perturbation Methods.* Cambridge University Press, Cambridge, 1991.

25. Bird, R.B., Stewart, W.E. & Lightfoot, E.N. *Transport Phenomena,* edn. 2 (Wiley, New York, 2002).

26. Leal, L.G. *Advanced Transport Phenomena: Fluid Mechanics and Convective Transport Processes* (Cambridge University Press, Cambridge, 2007).

27. Deen, W.M. 123. *Analysis of Transport Phenomena* (Oxford University Press, New York, 1998).

28. Squires, T.M. & Quake, S.R. Microfluidics: Fluid physics at the nanoliter scale. *Rev. Mod. Phys.* **77**, 977–1026 (2005).

29. Berg, H.C. *Random Walks in Biology* (Princeton University Press, Princeton, 1993).

30. Newman, J. The fundamental principles of current distribution and mass transport in electrochemical cells. in *Electroanalytical Chemistry* vol. 6 (ed. Bard, A.) 279–297, (Dekker, New York, 1973).

31. Ackerberg, R.C., Patel, R.D. & Gupta, S.K. Heat-mass transfer to a finite strip at small Peclet numbers. *J. Fluid Mech.* **86**, 49–65 (1978).

32. Zhang, W., Stone, H.A. & Sherwood, J.D. Mass transfer at a microelectrode in channel flow. *J. Phys. Chem.* **100**, 9462–9464 (1996).

33. Peluso, P. *et al.* Optimizing antibody immobilization strategies for the construction of protein microarrays. *Anal. Biochem.* **312**, 113–124 (2003).

34. Myszka, D.G., He, X., Dembo, M., Morton, T.A. & Goldstein, B. Extending the range of rate constants available from BIACORE: Interpreting mass transport-influenced binding data. *Biophys. J.* **75**, 583–594 (1998).

35. Schreiber, G. Kinetic studies of protein-protein interactions. *Curr. Opin. Struct. Biol.* **12**, 41–47 (2002).

36. Wallis, R., Moore, G.R., James, R. & Kleanthous, C. Protein-protein interactions in Colicin E9 Dnase-immunity protein complexes. 1. diffusion-controlled association and femtomolar binding for the cognate complex. *Biochemistry* **34**, 13743–13750 (1995).

37. Record, M.T., Zhang, W.T. & Anderson, C.F. Analysis of effects of salts and uncharged solutes on protein and nucleic acid equilibria and processes: a practical guide to recognizing and interpreting polyelectrolyte effects, Hofmeister effects, and osmotic effects of salts. in *Advances In Protein Chemistry,* vol. 51 (eds. Di Cera, E. & Eisenberg, D.E.) 281–353, (Academic Press, San Diego, 1998).

38. Belosludtsev, Y. *et al.* Nearly instantaneous, cation-independent, high selectivity nucleic acid hybridization to DNA microarrays. *Biochem. Biophys. Res. Commun.* **282**, 1263–1267 (2001).

39. Sosnowski, R.G., Tu, E., Butler, W.F., Oconnell, J.P. & Heller, M.J. Rapid determination of single base mismatch mutations in DNA hybrids by direct electric field control. *Proc. Natl. Acad. Sci. USA* **94**, 1119–1123 (1997).

40. Riggs, A.D., Bourgeoi, S. & Cohn, M. Lac repressor-operator interaction. III. kinetic studies. *J. Mol. Biol.* **53**, 401 (1970).

41. Wang, Y.M., Austin, R.H. & Cox, E.C. Single molecule measurements of repressor protein 1d diffusion on DNA. *Phys. Rev. Lett.* **97**, (2006).

42. Halford, S.E. & Marko, J.F. How do site-specific DNA-binding proteins find their targets? *Nucleic Acids Res.* **32**, 3040–3052 (2004).

43. Yoon, S.K., Fichtl, G.W. & Kenis, P.J.A. Active control of the depletion boundary layers in microfluidic electrochemical reactors. *Lab Chip* **6**, 1516–1524 (2006).

44. Vijayendran, R.A., Motsegood, K.M., Beebe, D.J. & Leckband, D.E. Evaluation of a three-dimensional micromixer in a surface-based biosensor. *Langmuir* **19**, 1824–1828 (2003).

45. Gervais, T. & Jensen, K.F. Mass transport and surface reactions in microfluidic systems. *Chem. Eng. Sci.* **61**, 1102–1121 (2006).